J Mater Sci (2011) 46:2324–2330
DOI 10.1007/s10853-010-5077-0

Dispersions of carbon nanotubes/polyhedral oligomeric silsesquioxanes hybrids in polymer: the mechanical, electrical and EMI shielding properties

Qi-Fang Li · Yihui Xu · Jin-San Yoon · Guang-Xin Chen

Received: 30 August 2010 / Accepted: 10 November 2010 / Published online: 30 November 2010

Abstract A hybrid was synthesized by grafting polyhedral oligomeric silsesquioxane (POSS) to multiwalled carbon nanotubes (MWCNTs). The MWCNT/polymer composites produced using silsesquioxane grafted MWCNTs as a filler had a high electromagnetic interference shielding effectiveness. Homogeneous dispersion of silsesquioxane grafted MWCNTs occurred throughout the polymer without any aggregation, while a pristine MWCNT aggregate that integrated several nanotube domains existed in the polymer matrix. A comparative study of the optical transmittance, electrical, and electromagnetic interference shielding properties of poly(L-lactide) (PLLA)/MWCNT composites based on pristine MWCNTs and silsesquioxane grafted MWCNTs was carried out. A high electromagnetic interference shielding effectiveness (15–16 dB) was obtained in the 36–50 GHz range at a relatively low filler loading (4 wt%) in the PLLA/silsesquioxane grafted MWCNT composite.

Introduction

Carbon nanotubes (CNTs) possess excellent mechanical, electrical, and thermal properties [1–4], but practical and economic difficulties arise when attempting to create devices and structures from pure CNTs. However, many of these limitations can be overcome by first dispersing the CNTs in a polymer matrix. This creates a number of advantages and provides a cost-effective substrate for the creation of novel materials or devices using CNTs. One benefit is that this type of polymer matrix can be readily processed, manipulated into shapes, and easily incorporated into devices. Second, by dispersing the expensive CNTs in a commodity polymer, it is possible to exploit the superior properties of the CNT at a more modest cost. Polymer/CNT composites promise superior mechanical, thermal, and electrical properties [5–8], but the manifestation of these superior properties depends on the extent of dispersion of the CNTs within the matrix. However, very often attaining a sufficient degree of dispersion is problematic.

Methods previously used to disperse CNTs and to create composites include procedures such as physical mixing of the CNTs with polymers [9], electrospinning [10], in situ polymerization in the presence of CNTs [11], surfactant-assisted processing of CNT/polymer composites [12], mechanochemical pulverization processes [13], the innovative latex fabrication method [14], coagulation spinning [15], solid-state shear pulverization [16], and ultrahigh-shear processing [17]. Since polymer composites using CNT as a filler were first reported in 1994 by Ajayan et al. [18], improving the dispersion has remained a challenge for scientists.

Among the various methods available, sidewall functionalization of CNTs with organic chains or functional groups is an effective way to improve the dispersion and strengthen the combination of CNTs with the polymer matrix [19, 20]. In the present study, we introduced an effective modifier in the form of polyhedral oligomeric silsesquioxanes (POSSs) with the formula $R_8Si_8O_{12}$ to functionalize the CNT sidewalls to improve the dispersion.

Q.-F. Li · Y. Xu · G.-X. Chen (✉)
Key Laboratory on Preparation and Processing of Novel Polymer Materials of Beijing, Beijing University of Chemical Technology, Beijing 100029, China
e-mail: gxchen@mail.buct.edu.cn

J.-S. Yoon
Department of Polymer Science and Engineering, Inha University, Incheon 402-751, Korea

The well-defined, almost cubic, silica-like core of POSS has a diameter of about 0.6 nm surrounded by eight reactive or inertia organic groups, which makes it topologically ideal for the preparation of intimate composite materials [21]. These molecules have been proposed for use as hard blocks or reinforcing particles in high performance polymer materials [22]. Polymers of this type show many improved properties over those with more traditional fillers, including excellent mechanical properties, higher usage temperatures, and increased fire retardance [23–27].

In this study, a mono-amino-POSS was chemically attached to a CNT by amidation reactions to produce a modified CNT (CNT-*g*-POSS). The other seven organic groups were exposed outside the CNT to provide a strong interaction between the CNT and the poly(L-lactide) (PLLA) matrix. PLLA was chosen as polymer matrix because of its biodegradable polymers which are now being used to replace the conventional synthetic plastics to reduce environmental pollution after disposal. The CNT-*g*-POSS was used to prepare polymer composites to study the electrical conductivity and electromagnetic interference (EMI) shielding effectiveness (SE) of this new CNT polymer.

Experimental methods

Materials

Multiwalled carbon nanotubes (MWCNTs) were a formulation provided by Aldrich, obtained by chemical vapor deposition and having a purity of >95%. The outer and inner diameters of the MWCNTs were 30–40 and 10–20 nm, respectively. The starting oxidation temperature of MWCNTs was 550 °C as measured by thermo gravimetric analysis under an air atmosphere. The bulk density of MWCNTs was 2.1 g/cm^3. Aminopropyl isooctyl-POSS was purchased from Hybrid Plastics and used without further purification. PLLA with a molecular weight of 1.7×10^5 g/mol used was obtained commercially and dried in a vacuum oven at 60 °C for 24 h before use.

Purification of MWCNTs

To remove the impurities such as metallic catalysts, in the MWCNTs, they were treated with 3 M HNO_3 and 1 M H_2SO_4 at 60 °C for 12 h, followed by a reflux process in 5 M HCl at 120 °C for 6 h. The purity of the acid-treated MWCNTs was measured at 99% by thermogravimetric analysis. These acid treatments shorten the length of MWCNTs and introduce carboxyl and hydroxyl groups into their structure (MWCNT-COOH).

Functionalization of MWCNT

The MWCNT-COOH preparation was reacted with excess $SOCl_2$ for 24 h under reflux, and then the residual $SOCl_2$ was removed by the reduced pressure distillation, to yield acyl chloride-functionalized MWCNTs (MWCNT-COCl). This MWCNT-COCl preparation was added to chloroform and the mixture was sonicated for 20 min to create a homogeneous dispersion. The mixture was then combined with the aminopropyl isooctyl-POSS under nitrogen, and the reactor was immersed in an oil bath at 70 °C and mechanically stirred for 72 h. The reacted mixture was then vacuum filtered through a 0.22 μm polycarbonate membrane and washed three times with excess chloroform to yield the pure MWCNT-*g*-POSS hybrid (Scheme 1).

Composite preparation

The composites of the PLLA/CNTs were prepared by melt compounding using a Brabender internal mixer at 180 °C for 4 min. The screw rotation speed is 60 rpm. The compounded and pelletized strands were dried under vacuum at 60 °C to remove the residual water. The dried pellets were then hot pressed at 180 °C for 1 min under 4 atm to form sheets with a thickness of approximately 0.4 mm. The molded sheets were then quickly cooled and annealed at 60 °C for 12 h, then used for various characterizations.

Measurements

The morphology of the composites was observed with a scanning electron microscope (SEM) (Hitachi S-4300) at an accelerating voltage of 5 kV after sputter coating the sample with a homogenous gold layer.

The grafting of POSS on MWCNT surface was characterized using a LEO922 in-column type energy-filtering transmission electron microscope (TEM) at an accelerating voltage of 200 kV with a LaB6 cathode equipped with an omega-type energy spectrometer. A detailed instrumental setup was described in our previous paper [28]. Oxygen elemental maps were created by a "two-window jump ratio" method, by selecting and using two recorded images

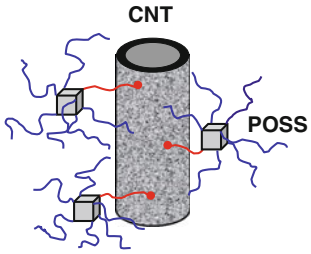

Scheme 1 Functionalization of the MWCNT with POSS

among those acquired by electron energy-loss spectroscopic imaging (image-EELS). The energy-filtered image beyond the silicon ionization edge at around 103 eV (post-edge image) was divided by the energy-filtered image below the ionization edge (pre-edge image). The energy position and the energy width of the two images used for the calculation of the elemental map were determined to obtain an elemental map with a high S/N ratio.

Raman spectra were measured with a laser Raman microscope (JASCO NRS-2100) using a 514.5 nm Ar line as the excitation source. The laser power was 0.5 W. The spectra were measured in a backscattering configuration with a triple monochromator at intervals of 1 cm^{-1}. The spatial resolution of the microscope was about 2 μm.

Thermo gravimetric analysis (TGA) was performed using a PL-TGA (Polymer Laboratories, TGA 1000, Shropshire, UK) by increasing the temperature from 30 to 900 °C at a heating rate of 20 °C/min in a nitrogen atmosphere.

Optical transmittances of the PLLA/CNTs films as well as neat PLLA were measured with a UV–visible spectrophotometer (UV-1650PC, Shimadzu, Japan).

An ADVANTEST R8340A ultrahigh-resistance meter was used to measure the high-resistance samples. Different applied voltages were used on different samples, depending on the level of resistivity of the specimen. Highly conductive samples caused short-circuiting of the equipment when the applied voltage was too great. The samples with high MWCNT concentrations were measured using a four-probe method, where current is applied through two contacts and voltage is measured across two other contacts.

The EMI SE was obtained according to the ASTM D-4935-99 method, using a network analyzer (Agilent, E8364B) equipped with an amplifier and a scattering parameter test set over a frequency range of 36 MHz–50 GHz. Samples were prepared with a punching machine and were installed into the test tool [29].

Results and discussion

Figure 1 shows the SEM images of the MWCNTs and MWCNT-*g*-POSSs after complete washing with chloroform. The presumption was made that only grafted POSSs were retained on the MWCNT surface. In the SEM images of the MWCNTs (Fig. 1a), the MWCNT walls are relatively smooth and clean and are not obviously covered with any extra phase. In contrast, the surfaces of MWCNT-*g*-POSS are clearly coated by a layer of POSS (Fig. 1b), and the average diameter has increased slightly compared with the raw MWCNT.

The energy-filtered TEM was used specifically to investigate the morphological structures of MWCNT-*g*-POSSs

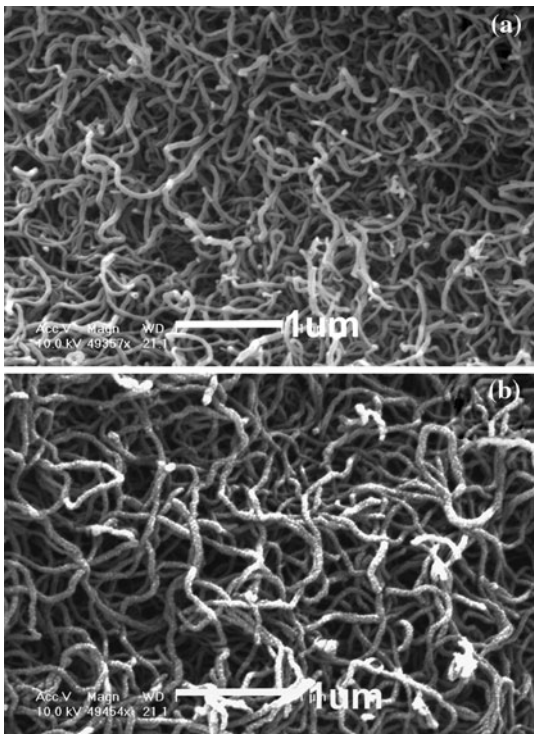

Fig. 1 SEM images of **a** MWCNT and **b** MWCNT-*g*-POSS

(Fig. 2). As shown in Fig. 2a, a zero-loss image of the MWCNT-*g*-POSS was formed by the unscattered and elastically scattered electrons with an energy range of 0 ± 10 eV. The MWCNT-*g*-POSS shown in Fig. 2a appears stained with an extra phase that is presumed to have mainly come from the grafted POSS molecules. This indicates that the grafting reaction had taken place not across the entire MWCNT surface and not just on the tips.

Image-EELS was performed in the energy ranges that included the silicon L2,3-ionization edges at around 103 eV. Figure 2b shows the silicon distribution images created by the three-window method, where the three appropriate energy-loss positions for the mapping were selected. As expected, the silicon distribution image (Fig. 2b) corresponds to POSS molecules bound to the MWCNT surface, while elemental silicon was not detected in the neat MWCNT surface. In other words, the energy-filtered TEM images showed direct evidence that POSS had become grafted onto the MWCNT surface.

The Raman spectra in Fig. 3 show the D- and G-bands of the MWCNT at 1350 and 1584 cm^{-1} for both MWCNT and MWCNT-*g*-POSS, which were attributed to the defects and disorder-induced peaks and the tangential-mode peaks, respectively [30]. These were the same as observed in the pristine nanotubes, which indicates that the electronic structure of the MWCNTs remained essentially unperturbed after the incorporation of POSS molecules. However, a smooth shoulder band located at 1622 cm^{-1}

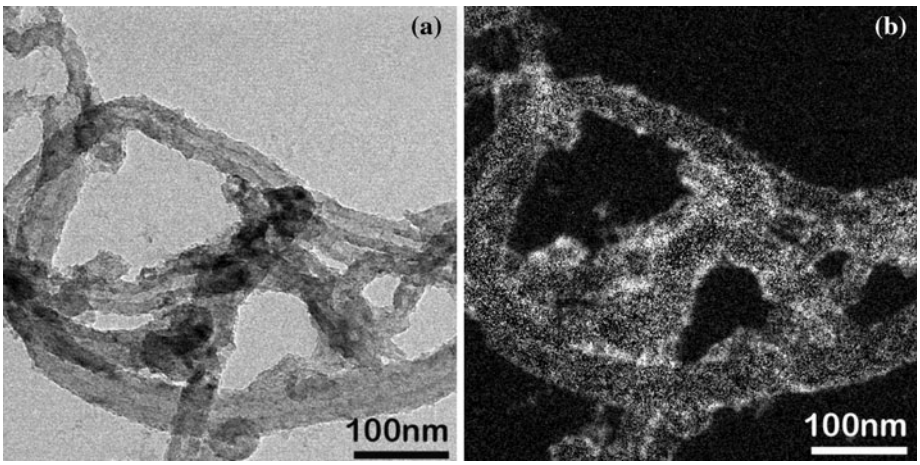

Fig. 2 Energy-filtering TEM imaging of MWCNT-*g*-POSS. **a** Zero-loss filtered image and **b** silicon distribution images

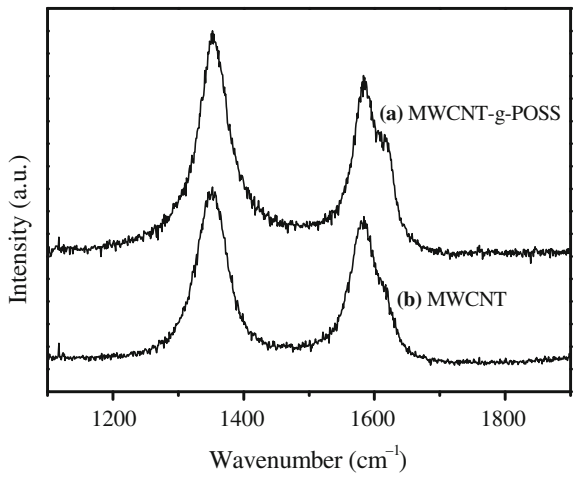

Fig. 3 Raman spectra of (*a*) MWCNT-*g*-POSS and (*b*) MWCNT

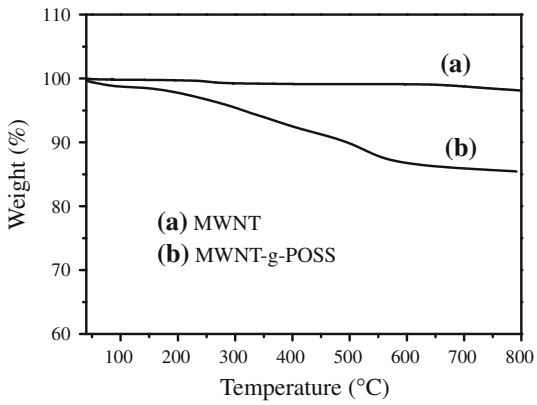

Fig. 4 TGA traces of (*a*) MWCNT and (*b*) MWCNT-*g*-POSS

was observed for the MWCNT-*g*-POSS. This peak has been attributed to sp2 hybridization of carbon and is evidence of the disruption of the aromatic system of p electrons by the attached molecules [31, 32]. The appearance of this obvious shoulder peak at 1622 cm^{-1} of the MWCNT-*g*-POSS samples demonstrated that organic molecules had been covalently attached.

The amount of the POSS grafted to the MWCNT was determined through the TGA analysis in a nitrogen atmosphere. The MWCNT-*g*-POSS exhibited a weight loss of about 12 wt% when the temperature was raised up to 800 °C due to the degradation of the alkyl structure of the grafted POSS on the MWCNT (Fig. 4). The amount of the POSS bound to the MWCNTs was calculated to be about 16 wt%.

SEM images of the fracture surface of MWCNT reinforced polymer composites, for evaluation of the dispersion of MWCNT in the polymer matrix and the interfacial interaction between the MWCNTs and polymer, are shown in Fig. 5. The cross-sections of PLLA/MWCNT-*g*-POSS and PLLA/MWCNT composites containing 1 wt% CNTs were made by fracturing the composites in liquid nitrogen to produce an intact fractured surface. The bright regions in the SEM images are attributed to MWCNTs as a result of their high electrical conductivity. Figure 5a shows that most of the MWCNTs are embedded within the PLLA matrix and that the MWCNTs show homogeneous dispersion in the PLLA matrix due to the interaction between MWCNT-*g*-POSSs and PLLA. The exfoliation of individual MWCNTs rather than aggregates is observed at the interface and most of these are broken rather than having been pulled out of the PLLA matrix. This observation suggests a relatively high interface interaction between the MWCNTs and the matrix. The aggregation of MWCNTs is prevented by the repulsion force produced by the coated POSS on the surface of MWCNTs.

The fracture interface for PLLA/MWCNT composites containing 1 wt% MWCNTs is also illustrated as a comparison of the efficiency in the exfoliation of MWCNTs in PLLA matrix. Figure 5b shows the SEM image of the fracture interface for PLLA composites containing raw MWCNTs. MWCNT aggregates integrating several individual nanotubes are found at the interface. This observation indicates that a well-dispersed PLLA/MWCNT

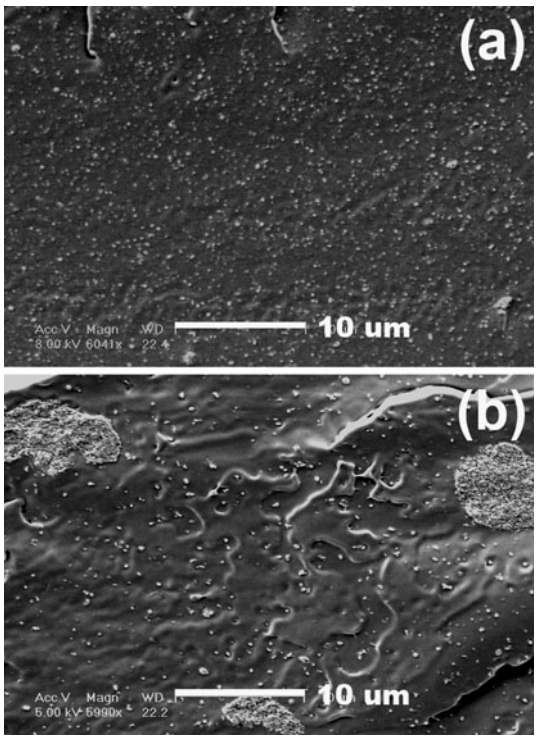

Fig. 5 SEM images of PLLA composites prepared via melt compounding **a** PLLA/MWCNT-*g*-POSS and **b** PLLA/MWCNT. The content of the MWCNTs was 1% by weight

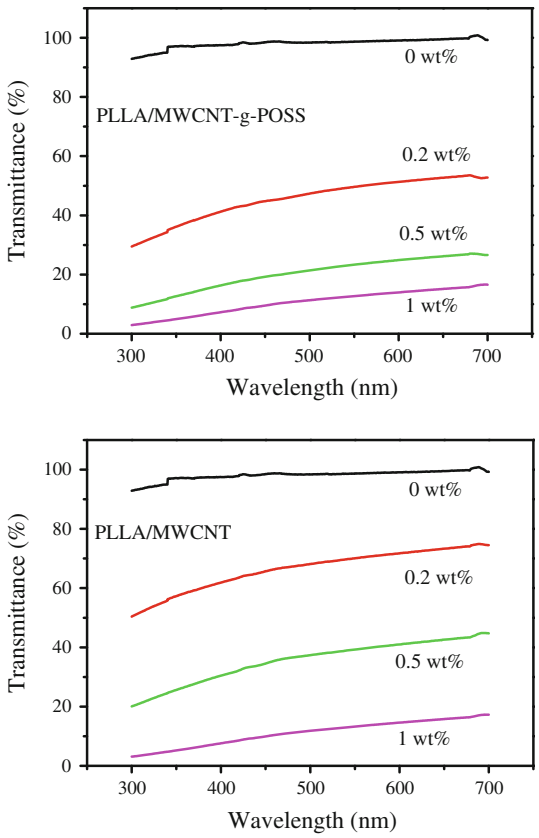

Fig. 6 Transmittance spectra for PLLA/MWCNT-*g*-POSS and PLLA/MWCNT composites films with varied nanotube loadings

composite cannot be obtained if raw MWCNTs are used as additives and that raw MWCNTs can be re-stacked together as aggregates. Therefore, the MWCNTs can easily slip out of the PLLA matrix due to their low interface interaction. The composites with poor nanotube dispersion have discrete nanotube-rich domains rather than a nanotube network.

The optical transmittances of neat PLLA, the PLLA/MWCNT and the PLLA/MWCNT-*g*-POSS composite films are shown in Fig. 6. The transmittance decreased as the CNT dispersion concentration increased. For the PLLA/MWCNT-*g*-POSS composite films, the optical transmittance gradually decreased as the wavelength decreased from 700 to 300 nm. A similar trend was observed for the PLLA/MWCNT composite. Comparison of the optical transmittances of PLLA/MWCNT-*g*-POSS and PLLA/MWCNT films in Fig. 6 shows that well-dispersed mixtures have a darker color upon visual observation, which should correspond to a lower transmittance intensity value. The low transmittance is due to the diffusion of light by the well-dispersed addictives in the composite films, indicating that the MWCNTs are very well dispersed. In the wavelength range of 300–700 nm, the optical transmittance of neat PLLA is around 98%. When the CNT loading was kept at 0.2 wt%, the PLLA/MWCNT samples exhibited 72% transmittance at 600 nm, whereas the PLLA/MWCNT-*g*-POSS samples showed about 52% transmittance. According to Fig. 6, the transmittance intensity of PLLA/MWCNT was higher than that of PLLA/MWCNT-*g*-POSS, which would agree with the order of the dispersion capability determined by SEM observation.

Figure 7 shows the representative stress–strain curves of neat PLLA, PLLA/MWCNT, and PLLA/MWCNT-*g*-POSS when 1 wt% of MWCNTs is added to PLLA. When the mechanical properties of PLLA/MWCNT are compared with those of neat PLLA, it reveals that the tensile strength and elongation at break of PLLA/MWCNT are significantly decreased as compared to those of neat PLLA, as shown in Fig. 7. This is attributed to poor dispersion of MWCNTs in PLLA/MWCNT and weak interfacial adhesion between MWCNTs and PLLA. However, the mechanical properties of composite are totally improved when the MWCNT-*g*-POSSs are incorporated into PLLA matrix, as can be seen in Fig. 7. Upon incorporation of 1 wt% of MWCNT-*g*-POSSs, the tensile modulus of PLLA goes up from 1598.0 to 2687.5 MPa and the yield strength is enhanced from 62.4 to 76.6 MPa indicating 68.2 and 22.7% improvements, respectively. The elongation at break of PLLA/MWCNT-*g*-POSS is not lower than that of neat PLLA. According to the enthalpy of melting, the

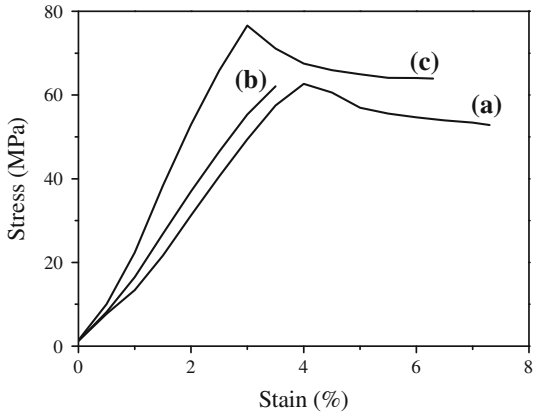

Fig. 7 Stress–strain curves of (*a*) PLLA, (*b*) simple blend of PLLA with 1 wt% of MWCNT, and (*c*) composite of PLLA with 1 wt% of MWCNT-*g*-POSS

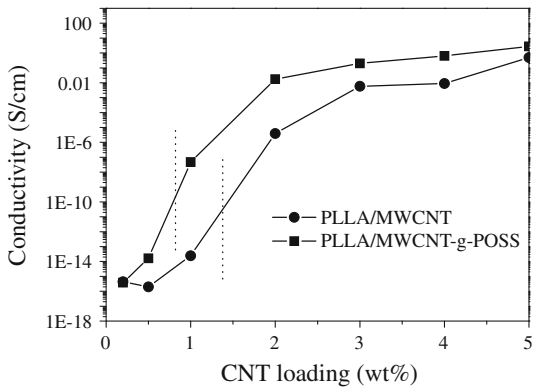

Fig. 8 Electrical conductivity of PLLA/MWCNT and PLLA/MWCNT-*g*-POSS composites as a function of nanotube loading

crystallinity of PLLA/MWCNT-*g*-POSS composites is slightly lower compared to that of neat PLLA. Therefore, the increased modulus and strength of the nanotube-containing composites are not attributed to the change in the crystallinity. It is thus believed that the strong interfacial adhesion is responsible for the enhancement of the mechanical properties.

The electrical conductivities of PLLA/MWCNT and PLLA/MWCNT-*g*-POSS are shown in Fig. 8. Comparison of the electrical conductivities of PLLA/MWCNT and PLLA/MWCNT-*g*-POSS indicated that the electrical conductivity of PLLA/MWCNT-*g*-POSS was higher than that of PLLA/MWCNT at all the MWCNT loadings. This suggested that the electrical conductivity of the composite was closely related to the dispersion of MWCNTs in polymer matrix. In other words, the better the dispersion of MWCNTs, the higher the electrical conductivity of polymer/MWCNT composites. An interesting observation was that the percolation threshold concentration became smaller with improved dispersion of MWCNTs: the electrical

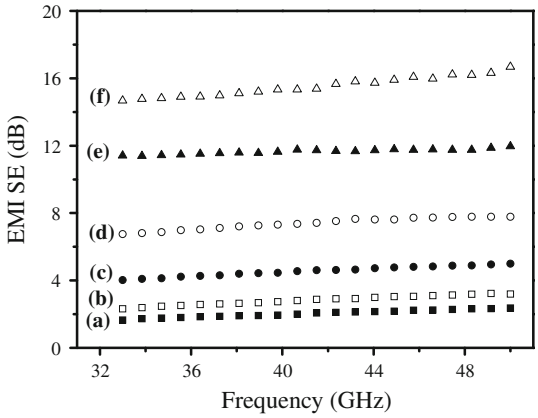

Fig. 9 EMI shielding effectiveness of PLLA/MWCNT (*a*) 0.5 wt %, (*c*) 1 wt%, (*e*) 4 wt% and PLLA/MWCNT-*g*-POSS (*b*) 0.5 wt%, (*d*) 1 wt%, (*f*) 4 wt% composites at the same thickness

conductivity of PLLA/MWCNT-*g*-POSS began to increase at 0.8 wt% MWCNT loading, while that of PLLA/MWCNT began to increase at 1.4 wt% MWCNT loading.

Figure 9 shows the EMI SE for both the PLLA/MWCNT and PLLA/MWCNT-*g*-POSS composites with 0.2–4 wt% MWCNT loadings. EMI performance for a conductor–insulator composite is related to the filler's intrinsic conductivity, dielectric constant, aspect ratio, and the dispersion [33–35]. SE increased with increasing MWCNT loading at a fixed frequency. At low loadings, the PLLA/CNT composites exhibited an almost frequency-independent EMI SE performance. At higher loadings, the EMI SE values tended to fluctuate more. The main contribution to the EMI shielding evidently came from the addition of the MWCNTs.

The PLLA/MWCNT-*g*-POSS composites showed better EMI shielding than did the PLLA/MWCNT composites. For example, the EMI SE of the PLLA/MWCNT-*g*-POSS composite with 4 wt% CNTs was 15 dB at 40 GHz, which was better than the 11 dB measured for the corresponding PLLA/MWCNT composite.

Even though the EMI SE of the composites increase with the increases in composite conductivity, some researchers believe that there is no scientific relationship between the two, since conductivity requires connectivity, while shielding does not [36]. Based on the experimental observations with MWCNTs and many other conductive fillers such as carbon black, vapor grown carbon nanofiber, metal fibers and grapheme, other researchers [37, 38] definitely claim that conductivity, and thereby connectivity, is required to produce a composite for EMI shielding. Therefore, more research is required to understand the relationship between the conductivity and the EMI SE of polymer composites.

In our results shown in Fig. 9, for samples of the same thickness and the same CNT loading, the increased EMI SE

in PLLA/MWCNT-*g*-POSS compared with the PLLA/MWCNT could be ascribed to the increase in the composite conductivity, which comes from the better dispersion of CNTs. It is worth mentioning here that these factors, such as filler intrinsic conductivity, distribution, and orientation, might have significant influence on the EMI shielding of a polymer composite. In our system, these factors were omitted since they are similar between MWCNT and MWCNT-*g*-POSS. More studies need to be done on SE and we hope to show more detailed data on this aspect in the near future.

Conclusions

MWCNTs were functionalized with aminopropyl isooctyl-POSS, creating novel MWCNT-*g*-POSS hybrids, which were characterized by SEM, Raman spectroscopy, energy-filtering TEM, and TGA. The hybrids provided a very good dispersion of nanotubes in the polymer matrix. The electrical threshold of PLLA/MWCNT-*g*-POSS composites was 0.8 wt%, which was lower than that of a raw MWCNT/PLLA composite at 1.4 wt%. POSS grafted onto MWCNTs results in better nanotube dispersion and less alignment of the nanotubes in the polymer, which leads to a higher mechanical properties, electrical conductivity, and EMI SE.

Acknowledgements The authors gratefully acknowledge financial support of this work coming from Natural Science Foundation of China (NSFC) (No. 21074009) and Young Foundation of Beijing University of Chemical Technology.

References

1. Calvert P (1999) Nature 399:210
2. Dresselhaus MS, Dresselhaus G, Saito R (1992) Phys Rev B 45:6234
3. Hone J, Llaguno MC, Biercuk MJ, Johnson AT, Batlogg B, Benes Z, Fischer JE (2002) Appl Phys A 74:339
4. Lourie O, Wagner HD (1998) J Mater Res 13:2418
5. Al-Saleh MH, Sundararaj U (2009) Carbon 47:2
6. Cao Q, Rogers JA (2009) Adv Mater 21:29
7. Park S, Choi IS (2009) Adv Mater 21:902
8. Wang S, Liang R, Wang B, Zhang C (2009) Carbon 47:53
9. Chen GX, Kim HS, Park BH, Yoon JS (2005) J Phys Chem B 109:22237
10. Sen R, Zhao B, Perea DE, Itkis ME, Hu H, Love J, Bekyarova E, Haddon RC (2004) Nano Lett 4:459
11. Chen GX, Kim HS, Park BH, Yoon JS (2006) Carbon 44:3373
12. Vigolo B, Poulin P, Lucas M, Launois P, Bernier P (2002) Appl Phys Lett 81:1210
13. Xia H, Wang Q, Li K, Hu GH (2004) J Appl Polym Sci 93:378
14. Regev O, ElKati PNB, Loos J, Koning CE (2004) Adv Mater 16:248
15. Vigolo B, Penicaud A, Coulon C, Sauder C, Pailler R, Journet C, Bernier P, Poulin P (2000) Science 290:1331
16. Furgiuele N, Lebovitz AH, Khait K, Torkelson JM (2000) Macromolecules 33:225
17. Chen G-X, Li Y, Shimizu H (2007) Carbon 45:2334
18. Ajayan PM, Stephan O, Colliex C, Trauth D (1994) Science 265:1212
19. Chen G-X, Kim H-S, Park BH, Yoon J-S (2007) Macromol Chem Phys 208:389
20. Lin Y, Hill DE, Bentley J, Allard LF, Sun Y-P (2003) J Phys Chem B 107:10453
21. Zhang C, Laine RM (2000) J Am Chem Soc 122:6979
22. Lichtenhan JD (1995) Comments Inorg Chem 17:115
23. Sellinger A, Laine RM (1996) Macromolecules 29:2327
24. Carroll JB, Frankamp BL, Srivastava S, Rotello VM (2004) J Mater Chem 14:690
25. Huang J, Xiao Y, Mya KY, Liu X, He C, Dai J, Siow YP (2004) J Mater Chem 14:2858
26. Lee J, Cho H-J, Cho NS, Hwang D-H, Shim H-K (2006) Synth Met 156:590
27. Matejka L, Strachota A, Plestil J, Whelan P, Steinhart M, Slouf M (2004) Macromolecules 37:9449
28. Chen G-X, Shimizu H (2008) Polymer 49:943
29. Wu J, Chung DDL (2002) Carbon 40:445
30. Jorio A, Pimenta MA, Souza Filho AG, Saito R, Dresselhaus G, Dresselhaus MS (2003) New J Phys 5:139.1
31. Wu H-X, Qiu X-Q, Cao W-M, Lin Y-H, Cai R-F, Qian S-X (2007) Carbon 45:2866
32. Wu H-X, Tong R, Qiu X-Q, Yang H-F, Lin Y-H, Cai R-F, Qian S-X (2007) Carbon 45:152
33. Chung DDL (2001) Carbon 39:279
34. Huang Y, Li N, Ma Y, Du F, Li F, He X, Lin X, Gao H, Chen Y (2007) Carbon 45:1614
35. Liu Z, Bai G, Huang Y, Ma Y, Du F, Li F, Guo T, Chen Y (2007) Carbon 45:821
36. Yang S, Lozano K, Lomeli A, Foltz HD, Jones R (2005) Composites Part A 36:691
37. Al-Saleh MH, Sundararaj U (2009) Carbon 47:1738
38. Liang J, Wang Y, Huang Y, Ma Y, Liu Z, Cai J, Zhang C, Gao H, Chen Y (2009) Carbon 47:922